Contributions of a Higher Triplet Excited State to the Emission Properties of a Thermally Activated Delayed-Fluorescence Emitter

Takashi Kobayashi,[1,2,*] Akitsugu Niwa,[1] Kensho Takaki,[1] Shota Haseyama,[1] Takashi Nagase,[1,2] Kenichi Goushi,[3,4,5] Chihaya Adachi,[3,4,5] and Hiroyoshi Naito[1,2,†]

[1]*Department of Physics and Electronics, Osaka Prefecture University, 1-1 Gakuencho, Naka, Sakai 599-8531, Japan*

[2]*Research Institute of Molecular Electronic Devices (RIMED), Osaka Prefecture University, 1-1 Gakuencho, Naka, Sakai 599-8531, Japan*

[3]*Center for Organic Photonics and Electronics Research (OPERA), Kyushu University, 744 Motooka, Nishi, Fukuoka 819-0395, Japan*

[4]*Japan Science and Technology Agency (JST), ERATO, Adachi Molecular Exciton Engineering Project, 744 Motooka, Nishi, Fukuoka 819-0395, Japan*

[5]*International Institute for Carbon Neutral Energy Research (WPI-I2CNER), Kyushu University, 744 Motooka, Nishi, Fukuoka 819-0395, Japan*

(Received 23 August 2016; revised manuscript received 7 January 2017; published 6 March 2017)

The temperature dependences of photoluminescence (PL) decay rates and the PL spectrum of a thermally activated delayed-fluorescence emitter, 1,2,3,5-tetrakis(carbazol-9-yl)-4,6-dicyanobenzene (4CzIPN), are investigated. It is found that not only the lowest singlet (S_1) and triplet (T_1) excited states but also an additional triplet excited state (T_n) lying between S_1 and T_1 play an important role in the exciton decay process, particularly around 100 K. At around this temperature, some of the triplet excitons are thermally activated into T_n but not up to S_1, and they then decay into the ground state (S_0) with phosphorescence emission. Therefore, two kinds of phosphorescence, originating from T_n and T_1, are observed. The temperature dependence of the PL decay rates of 4CzIPN can be explained by a four-level model consisting of S_1, T_1, T_n, and S_0, and its energy gaps between T_n and T_1 and between S_1 and T_1 are determined to be 45 ± 5 meV and 135 ± 10 meV, respectively.

DOI: 10.1103/PhysRevApplied.7.034002

I. INTRODUCTION

Recently, molecules that exhibit thermally activated delayed fluorescence (TADF) have attracted considerable attention as alternative emitters for organic light-emitting diodes (OLEDs) [1]. In TADF emitters, excitons in the lowest triplet excited state (T_1) can be activated into the lowest singlet excited state (S_1) by thermal energy at room temperature and then decay into the ground state (S_0) with delayed-fluorescence emission. Thus, in OLEDs using TADF emitters, triplet excitons created after recombination of injected electrons and holes can be converted into photons without expensive phosphorescence emitters [2]. To obtain efficient TADF, the energy gap between S_1 and T_1 (ΔE_{st}) should be small enough that triplet excitons can populate the S_1 level at room temperature. The main strategy to realize a small ΔE_{st} is to use molecules that have an intramolecular charge-transfer (CT) excited state as S_1. In such molecules, the spatial overlap between wave functions of the CT excited state and the ground state is limited, resulting in a considerable reduction of the exchange integral and, consequently, a small singlet-triplet energy splitting [3,4]. Based on this design principle, a series of carbazolyl-dicyanobenzene-based CT molecules have been synthesized, and it has been confirmed that they exhibit efficient TADF. In addition, using one of those TADF emitters—i.e., 1,2,3,5-tetrakis(carbazol-9-yl)-4,6-dicyanobenzene (4CzIPN)—OLEDs with an excellent external quantum efficiency (19%), comparable to phosphorescence emitters, has been demonstrated [2].

As mentioned above, the basics of exciton decay dynamics in TADF emitters has frequently been explained only in terms of S_1, T_1, and S_0 [5,6]. Such a simple explanation seems to be sufficient because, according to Kasha's rule [7], excitons created in higher excited states are expected to decay immediately into S_1 or T_1. As is well known, for some CT molecules in solution, more excited states, e.g., locally excited (LE) states, should be considered. Depending on the polarity of the solvent, the order of the lowest singlet CT and LE states may be reversed, and, consequently, their emission properties are dramatically changed [8,9]. In these studies, however, attention has still been paid only to the lowest excited state. Recently, the importance of a higher triplet excited state than T_1 (hereafter abbreviated as T_n) in an exciton decay process in a TADF emitter was pointed out [10–15]. Specifically, Dias *et al.* found that activation rates from the lowest CT state

*tkobaya@pe.osakafu-u.ac.jp
†naito@pe.osakafu-u.ac.jp

and the lowest LE state into S_1 are different, so that the efficiency of TADF is largely dependent on the solvent polarity [13]. Their findings indicate that, in some TADF emitters, the TADF efficiency is determined not only by the ΔE_{st} value but also by the order of the lowest two triplet excited states. It therefore seems to be essential to consider T_n as well as S_1, T_1, and S_0 in order to better understand the exciton decay dynamics.

Since the demonstration of the excellent external quantum efficiency of OLEDs using 4CzIPN [2], various optoelectronic properties of 4CzIPN have been investigated [2,16–22]. However, it is still unclear whether 4CzIPN has such a T_n between S_1 and T_1 and, if it does, how important T_n is in its exciton decay dynamics. In this work, we apply a three-level model consisting only of S_1, T_1, and S_0, and a four-level model also including T_n to the temperature dependence of the photoluminescence (PL) properties of 4CzIPN-doped thin films. It is found that the observed temperature dependence of the PL decay rates is inconsistent with expectations from the three-level model, but it can be well explained by the four-level model. In addition, the PL of 4CzIPN around 100 K contains a component that is attributable to phosphorescence from T_n. We therefore have concluded that 4CzIPN indeed has a T_n state which influences the exciton decay process.

II. EXPERIMENT

In this work, 4CzIPN-doped thin films are fabricated on sapphire substrates via spin coating from a dichloromethane solution in which 4CzIPN and a host material, 1,3-bis (9-carbazolyl)benzene, are dissolved in a 5:95 weight ratio. During the measurements, the samples are maintained in a vacuum (10^{-3} Pa) in a closed-cycle helium cryostat. For PL measurements, the samples are excited by pulses of the third-harmonic wavelength (355 nm) of a Nd:yttrium aluminum garnet laser. To avoid unfavorable influences due to exciton-exciton annihilation processes such as triplet-triplet and singlet-triplet annihilations [17], we set the pulse energy density to be less than 100 μJ cm^{-2} pulse^{-1} and the repetition rate to be less than 1 Hz. With a pair of lenses, PL from the sample is collected and led to a monochromator. The PL decay curves over a short time range until 150 ns after the pulsed excitation are recorded with an oscilloscope connected to a gigahertz amplified photodiode. The time resolution of the setup is a few nanoseconds. On the other hand, PL decay curves over a longer time range are recorded with a photon-counting system and a photomultiplier tube. We also use a mechanical shutter to prevent the initial intense part of the PL decay from entering the photomultiplier tube. The PL spectra are measured using a CCD detector coupled to the monochromator using a relatively long integration time (1 s) comparable to the time interval between the adjacent laser pulses. Phosphorescence spectra are measured by starting the integration 30 ms after the incidence of the laser pulse.

III. RESULTS

A. Temperature dependence of decay rates

Figure 1 shows the normalized time-integrated PL and phosphorescence spectra at 7 K. The time-integrated PL of 4CzIPN may contain several PL components, such as fluorescence and phosphorescence. At room temperature, PL exclusively originates from S_1 so that the measured time-integrated PL spectrum can be regarded as the fluorescence spectrum, although the phosphorescence spectrum at this temperature cannot be recorded. On the other hand, at very low temperatures, the phosphorescence spectrum can be recorded, as shown in Fig. 1, whereas the fluorescence spectrum at these temperatures cannot be measured separately from the phosphorescence; a phosphorescence component is always included, even in a time-resolved PL spectrum. Usually, ΔE_{st} is estimated from a comparison between the fluorescence and phosphorescence spectra [4,5]. For the case of 4CzIPN, in addition to the difficulty in knowing both of the fluorescence and phosphorescence spectral shapes at any temperatures, these spectra must be too broad to determine its small ΔE_{st}.

As shown later (Fig. 6), the time-integrated PL spectrum has a peak of around 2.4 eV at any temperatures between 7 and 300 K. Thus, we measure temporal evolutions of PL intensity at 2.4 eV. Figure 2(a) shows PL decay curves measured at 7 and 300 K in the short time range. In this time range, the temperature dependence of the PL decay curve is not strong, and PL always decays nonexponentially. Here, we define a decay rate for this short time range as the reciprocal of the time required for the PL to decrease to $1/e$ of its initial value, where e is the base of the natural logarithm. The determined decay rates are around 3×10^7 s^{-1}, as shown in Fig. 2(b).

In contrast, PL decay curves in the long time range are strongly dependent on temperature. The PL decay curves measured at 7 and 300 K are shown in Figs. 3(a) and 3(b), respectively. At 7 K, the tail of the PL decay curve reaches 2 s.

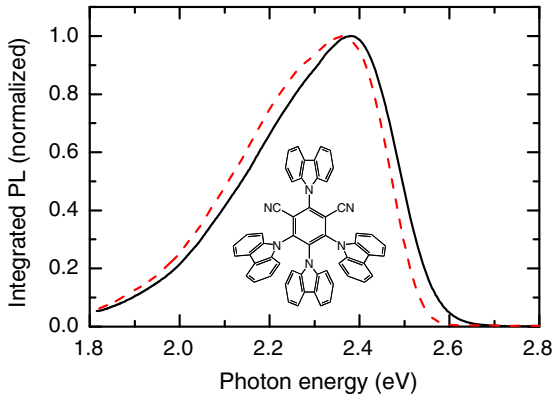

FIG. 1. The solid and dashed lines are normalized time-integrated PL and phosphorescence spectra at 7 K, respectively. (Inset) The chemical structure of 4CzIPN.

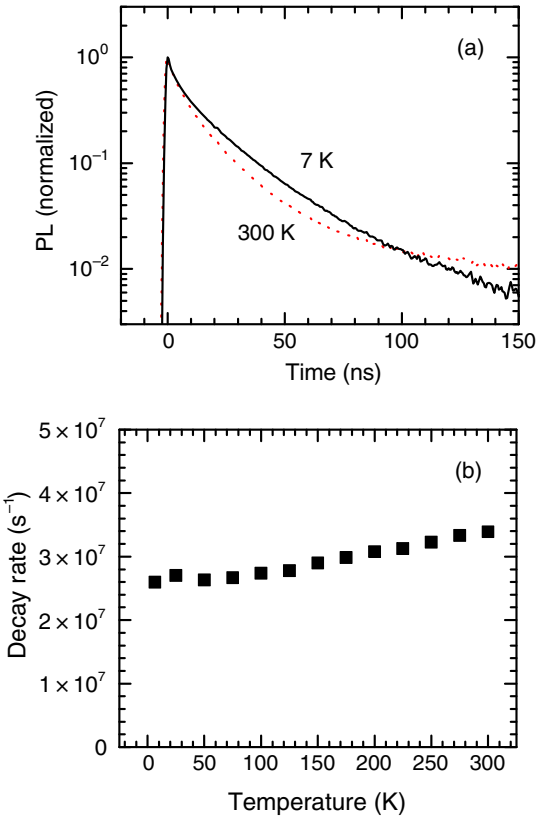

FIG. 2. (a) Solid and dotted lines represent PL decay curves at 7 and 300 K. (b) Temperature dependence of the decay rate estimated from the decay curves in the short time range.

These curves cannot be fitted with a single exponential function, even if the initial part of the curves in the short time range are ignored. Thus, we obtain the decay rate for the long time range as follows: we first fit a sum of three exponential functions to the curve at 300 K and regard the lowest estimated decay rate as the decay rate for the long time range. Then we fit a sum of several exponential functions to the curve at a lower temperature and choose the decay rate that is continuously connected to the estimated decay rates for the higher temperatures. The reason why we focus on the lowest decay rate is that the lower decay rate is more sensitive to temperature and is expected to be less influenced by the exciton-exciton annihilation processes. The estimated decay rates for the long time range are shown in Fig. 3(c). Note that, although these decay rates are slightly dependent on the method used to estimate, the change is tiny compared to the huge variations by 5 orders of magnitude due to a temperature change.

Before discussion of the four-level model, we apply the three-level model to interpret the experimental results. The assumed energy diagram is illustrated in Fig. 4(a). Based on the three-level model, the time evolution of S_1 and T_1 exciton densities can be described by rate equations that can be analytically solved. The solutions for the S_1 and T_1

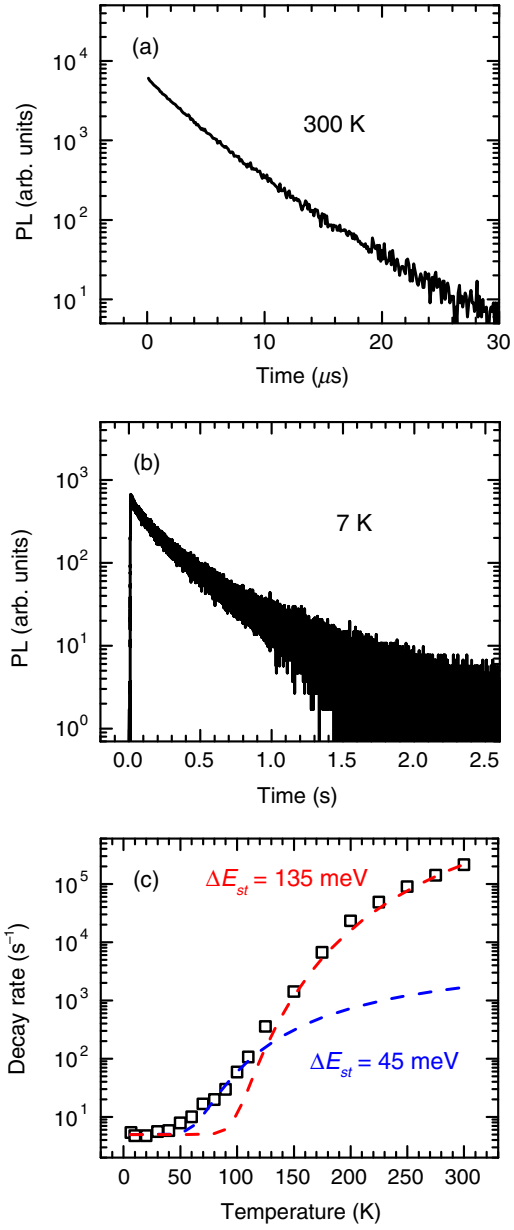

FIG. 3. PL decay curves at (a) 300 K and (b) 7 K. (c) The temperature dependence of the estimated decay rate for the long time range. The blue and red dashed lines are fitted results based on a three-level mode with ΔE_{st} of 45 and 135 meV, respectively.

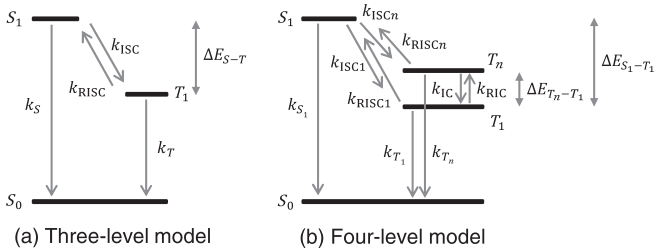

FIG. 4. The assumed energy diagrams of (a) a three-level model and (b) a foul-level model.

exciton densities both have the form of a sum of two exponential functions [23,24]. This indicates that the PL decay curve consists of fast (prompt) and slow (delayed) components. Although the experimental decay curves cannot be fitted with a sum of two exponential functions, we assume here that, within the framework of the three-level model, the decay rates determined for the long time range shown in Fig. 3(c) correspond to the delayed component. From the analytic solutions of the rate equations [23,24], the decay rate of the delayed component (k_d) is given by

$$k_d = \frac{1}{2}\left\{k_S + k_{\mathrm{ISC}} + k_{\mathrm{RISC}} + k_T - \sqrt{(k_S + k_{\mathrm{ISC}} + k_{\mathrm{RISC}} + k_T)^2 - 4[k_{\mathrm{ISC}}k_T + k_S(k_{\mathrm{RISC}} + k_T)]}\right\}, \tag{1}$$

where k_S and k_T are decay rates from S_1 and T_1, respectively, and k_{ISC} and k_{RISC} are rates for intersystem crossing (ISC) and reverse ISC (RISC), respectively. If we assume that a population of an excited state is described by a Boltzmann distribution, k_{RISC} can be written as

$$k_{\mathrm{RISC}} = k_{\mathrm{ISC}} \exp\left(-\frac{\Delta E_{st}}{k_B T}\right), \tag{2}$$

where k_B is the Boltzmann constant and T is the temperature. Thus, using Eqs. (1) and (2), the temperature dependence of k_d can be calculated. However, the experimental decay rates cannot be reproduced with Eq. (1). In Fig. 3(c), we show two examples of the calculated results. One result obtained with ΔE_{st} of 45 meV reproduces the gradual onset at around 50 K, but the expected decay rate at 300 K is 2 orders of magnitude lower than the experimental value. In the other result, with ΔE_{st} of 135 meV, the deviation at around 100 K is remarkable. The decay rates in the entire measured temperature range cannot be reproduced with any single ΔE_{st} value with the three-level model. Note that the discrepancy is not due to the omission of the temperature dependences of k_S, k_T, and k_{ISC}. The first two are confirmed to be temperature independent from the fact that the PL quantum efficiency (PLQE) of 4CzIPN is almost constant if it is measured with a sufficiently weak excitation laser in order to avoid the exciton-exciton annihilation processes [21]. The temperature dependence of k_{ISC} must also be weak; if not, the decay rate in Fig. 2(a) should exhibit a much stronger temperature dependence.

In the case of a four-level model also including T_n, the time evolution of the exciton densities in S_1, T_n, and T_1 are described by the following rate equations:

$$\begin{aligned}
\frac{dS_1(t)}{dt} &= G - (k_S + k_{\mathrm{ISC}n} + k_{\mathrm{ISC1}})S_1 + k_{\mathrm{RISC}n}T_n + k_{\mathrm{RISC1}}T_1,\\
\frac{dT_n(t)}{dt} &= k_{\mathrm{ISC}n}S_1 - (k_{T_n} + k_{\mathrm{IC}} + k_{\mathrm{RISC}n})T_n + k_{\mathrm{RIC}}T_1,\\
\frac{dT_1(t)}{dt} &= k_{\mathrm{ISC}_1}S_1 + k_{\mathrm{IC}}T_n - (k_{T_1} + k_{\mathrm{RISC1}} + k_{\mathrm{RIC}})T_1,
\end{aligned} \tag{3}$$

where G represents the generation rate of singlet excitons by the excitation light and k_{IC} is the rate of internal conversion, and the rates with n and 1 in the subscript are associated with T_n and T_1, respectively, and R in the subscript indicates the reverse processes. The assumed energy diagram is shown in Fig. 4(b). The rate equations can be solved using a Laplace transform (see the Appendix). The time evolution of S_1, T_n, and T_1 are given in the form of a sum of three exponential functions:

$$S_1, T_n, T_1 = A\exp(-k_1 t) + B\exp(-k_2 t) + C\exp(-k_3 t), \tag{4}$$

where A, B, and C are determined by the initial conditions (see the Appendix). The characteristic decay rates k_1, k_2, and k_3 are common for S_1, T_n, and T_1, and can be obtained as solutions of a cubic equation [see Eq. (A3) in the Appendix]. By analogy with the three-level mode, k_1, k_2, and k_3 correspond to decay rates of excitons in S_1, T_n, and T_1, respectively, in a situation where the thermal activation processes can be ignored. Although the excitons in S_1 always decay downward, excitons in T_n and T_1 can decay upward through higher states as well. It is thus expected that k_2 and k_3 are dependent on temperature, whereas k_1 is temperature independent. Using Eq. (A3) in the Appendix, the temperature dependence of the three decay rates can be calculated if we assume the Boltzmann distribution, i.e., the following relationships:

$$\begin{aligned}
k_{\mathrm{RISC}n} &= k_{\mathrm{ISC}n}\exp\left(-\frac{\Delta E_{S_1-T_1} - \Delta E_{T_n-T_1}}{k_B T}\right),\\
k_{\mathrm{RISC1}} &= k_{\mathrm{ISC1}}\exp\left(-\frac{\Delta E_{S_1-T_1}}{k_B T}\right),\\
k_{\mathrm{RIC}} &= k_{\mathrm{IC}}\exp\left(-\frac{\Delta E_{T_n-T_1}}{k_B T}\right).
\end{aligned} \tag{5}$$

One example of the calculated temperature dependence of the three decay rates is shown in Fig. 5. In Table I, we list the physical constants that are used to obtain the example. The calculated lowest decay rate almost

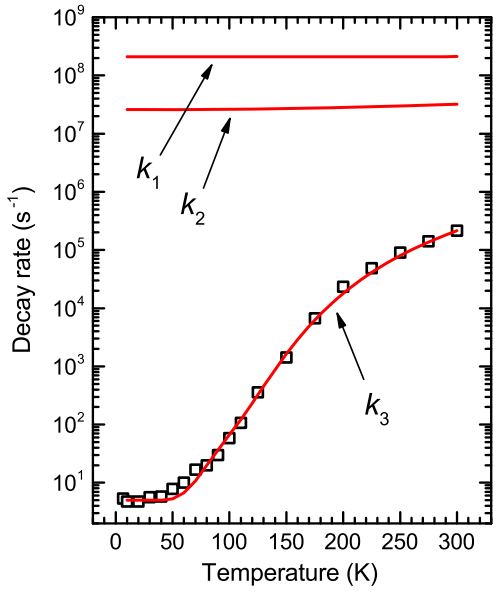

FIG. 5. Temperature dependence of three decay rates, k_1, k_2, and k_3 in Eq. (4), calculated based on the four-level model. The open squares are the experimental decay rates for the data shown in Fig. 3(c).

completely reproduces the experimental temperature dependence of the decay rate. The calculated highest decay rate is virtually independent of temperature, whereas the middle decay rate slightly increases with increasing temperature. The latter feature is consistent with the experimental result shown in Fig. 2(b). We therefore conclude that the four-level model is much more suitable for explaining the temperature dependence of the decay rates than the three-level model. It should be noted that the highest decay rate may be too fast to be measured with our experimental setup or may be omitted because of the way we determine a decay rate for the short time range. In spite of the good agreement between the experimental and calculated results, it is impossible to determine all of the constants in Table I using this calculation. Similar calculation results can be obtained with different sets of constants; for instance, when one of k_{S_1}, $k_{\mathrm{ISC}n}$, and k_{ISC1} increases and the others decrease, almost the same result will be obtained. Although the k_{S_1}, $k_{\mathrm{ISC}n}$, and k_{ISC1} values in Table I seem to be large for a TADF emitter [2], the experimental lowest decay rate at room temperature cannot be reproduced if all of the three decay rates are reduced. The sum of the three seems to be a kind of true variable. From the calculations, only the k_{T_1} and k_{IC} values can be uniquely determined; the latter is nearly equal to the middle decay rate at 7 K as far as we examined. However, to obtain good agreement between the calculated and experimental results, the energy gap between T_n and T_1 ($\Delta E_{T_n-T_1}$) should be 45 ± 5 meV and the energy gap between S_1 and T_1 ($\Delta E_{S_1-T_1}$) should be 135 ± 10 meV. In other words, these energy gaps are strongly suggested from the calculations. This $\Delta E_{T_n-T_1}$ value is almost the same as the activation energy that we previously estimated as a major activation energy in 4CzIPN from the temperature dependence of its PLQE [17]. Below 100 K, the PLQE of 4CzIPN is largely reduced because of the exciton-exciton annihilation processes. In such a low-temperature region, as a result of the suppression of the activation process, the triplet exciton density significantly increases under a continuous-wave photoexcitation and thus the exciton-exciton annihilation processes are accelerated. In our previous work [17], we estimated the activation energy by analyzing the temperature dependence of the PLQE using a theoretical relationship between the PLQE and the temperature that is derived based on the three-level model. In the model, the higher excited state is essential for modeling the thermal activation process from the lower excited state, but it is not needed to be a singlet. Thus, the activation energy that we previously estimated [17] must correspond to $\Delta E_{T_n-T_1}$. In fact, the temperature dependence of the PLQE can also be reproduced using the four-level model with $\Delta E_{T_n-T_1} = 45 \pm 5$ meV and $\Delta E_{S_1-T_1} = 135 \pm 10$ meV.

TABLE I. Physical constants used to calculate the temperature dependence of the PL decay rates in Fig. 5.

Constants	Values
k_S	7×10^7 s^{-1}
k_{IC}	2.6×10^7 s^{-1}
k_{T_1}	5 s^{-1}
k_{T_n}	1×10^4 s^{-1}
k_{ISC1}	7×10^7 s^{-1}
$k_{\mathrm{ISC}n}$	7×10^7 s^{-1}
$\Delta E_{T_n-T_1}$	45 ± 5 meV
$\Delta E_{S_1-T_1}$	135 ± 10 meV

With the four-level model, the temperature dependence of the decay rates in Fig. 5 can be understood as follows: at very low temperatures, the triplet excitons in T_1 have to decay into S_0 with emission of the phosphorescence and its decay rate, which corresponds to k_{T_1}, is only a few s^{-1}. As temperature increases, the triplet excitons start decaying through T_n into S_0. There must be a temperature region where the triplet exciton can be activated into T_n but not up to S_1, so that the triplet excitons preferentially decay through T_n. If such a temperature region did not exist, the four-level model should not be needed to explain the temperature dependence of the decay rates, and the three-level model should be sufficient. The necessity for the four-level model indicates the importance of T_n in the exciton decay process in 4CzIPN. In Fig. 3(c), we show the calculated result based on the three-level model for ΔE_{st} of 135 meV, which is equal to the estimated $\Delta E_{S_1-T_1}$ value.

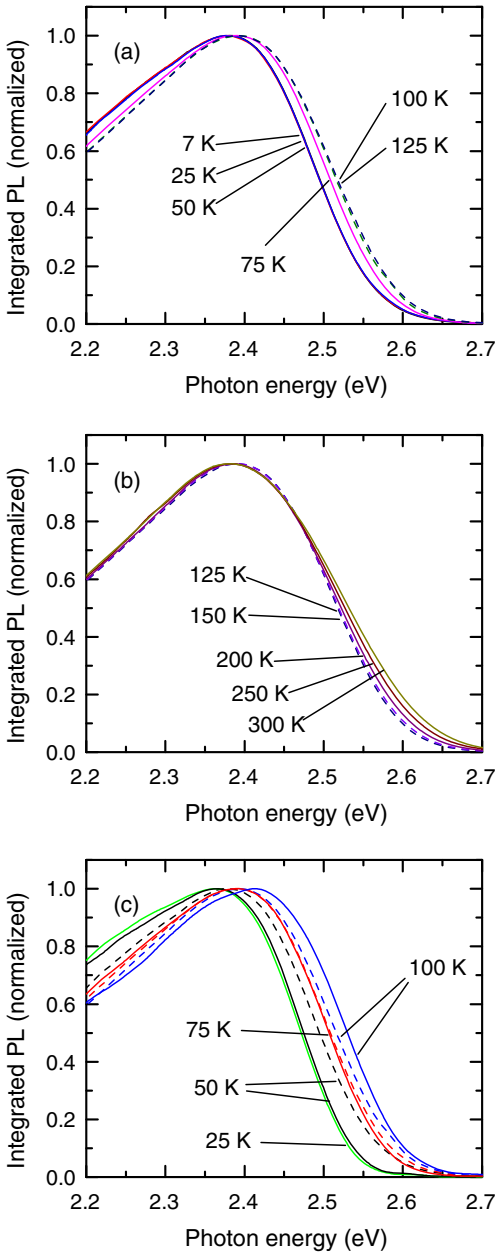

FIG. 6. Time-integrated PL spectra of 4CzIPN measured at various temperatures (a) from 7 to 125 K and (b) from 125 to 300 K. In (a) and (b), some spectra are indicated by dashed lines for clarity. (c) Solid lines are phosphorescence spectra measured at 25, 50, 75, and 100 K, whereas the dashed lines are the time-integrated PL spectra at 50, 75, and 100 K. The time-integrated PL spectra in (c) are the same as in (a).

From the discrepancy between the calculated and experimental results in Fig. 3(c), it is expected that the contribution of T_n is maximized at around 100 K, where the experimental decay rate, 30 s^{-1}, is one order magnitude larger than k_{T_1} [see Fig. 3(c)]. At even higher temperatures, a larger number of triplet excitons decay through S_1. At 300 K, the experimental decay rate reaches 2.1×10^5 s^{-1},

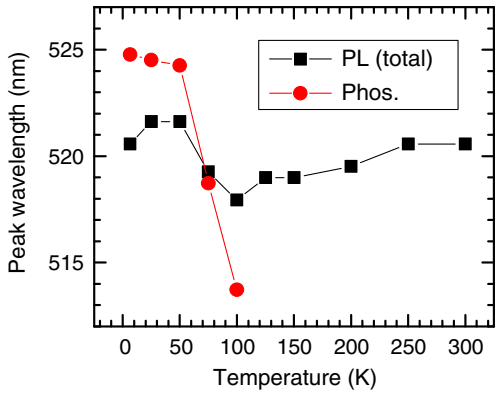

FIG. 7. Temperature dependence of the peak photon energies of the time-integrated PL and the phosphorescence.

and thus the direct decay from T_1 and T_n into S_0 is negligible at this temperature.

The above scenario may raise a question regarding the exciton decay process: is the transition from T_n into S_0 radiative or nonradiative? As mentioned above, the PLQE of 4CzIPN remains high between 7 and 300 K when it is measured with a sufficiently weak excitation laser [21]. Therefore, the decay from T_n into S_0 can be identified as radiative. If so, the phosphorescence component originating from T_n should be contained in the observed PL. In the next section, we investigate the temperature dependence of the PL spectrum to find this phosphorescence component.

B. Temperature dependence of the PL spectrum

Figures 6(a) and 6(b) are the time-integrated PL spectra measured at various temperatures below and above 125 K, respectively. The spectrum does not change at all below 50 K, and it slightly broadens with increasing temperatures above 100 K. The remarkable spectral shift of 20 meV is observed only between 50 and 100 K. This spectral shift can be more clearly recognized in Fig. 7, where the peak photon energy is plotted as a function of the temperature. The spectral shift of the time-integrated PL is due to the shift of phosphorescence, which shifts by 50 meV around the same temperature region, as shown in Figs. 6(c) and 7. Unfortunately, the phosphorescence spectrum cannot be measured above 100 K because its decay rate becomes too fast to be measured separately from the fluorescence component using a mechanical shutter. No further spectral shift of the phosphorescence is, however, expected above 100 K from the fact that the time-integrated PL does not shift above 100 K. Between 7 and 100 K, the spectral broadening suggestive of the influence of molecular vibrations is not apparent (see Fig. 6). Thus, the spectral shift can be considered to result from a switch from phosphorescence from T_1 at a lower temperature side into another PL component at a higher temperature side. The latter PL component is observed at 100 K, where the triplet excitons cannot be activated up to S_1. Furthermore, the spectral shift

of 50 meV is almost the same as the $\Delta E_{T_n-T_1}$ value estimated above. Therefore, we assign the blueshifted phosphorescence observed at around 100 K to phosphorescence originating from T_n.

From Figs. 6(c) and 7, it is found that, at 100 K, the peak of the phosphorescence from T_n appears at higher photon energies than that of the time-integrated PL. This blueshifted peak of the phosphorescence does not mean that T_n lies higher in energy than S_1. It simply results from the steeper onset of the phosphorescence from T_n than that of the fluorescence from S_1. Since S_1 is a CT excited state, it is reasonable that fluorescence from S_1 has a broad spectral shape. The narrower spectral shape of the phosphorescence components from T_1 as well as T_n suggests that these triplet excited states have less CT character than S_1, and that they may be LE states. The spectral difference between the fluorescence from S_1 and the phosphorescence from T_n is also a key to understanding the spectral broadening of the time-integrated PL shown in Fig. 6(b): as temperature increases, thermal activation into S_1 is accelerated so that the broad fluorescence component from S_1 relatively increases, whereas the narrower phosphorescence component from T_n decreases. As a result, the time-integrated PL seems to be broadened with increasing temperature.

IV. DISCUSSION

It is technically impossible to measure the fluorescence and the two phosphorescence spectra separately from one another. Thus, the relative ratio between the three PL components cannot be experimentally determined. Instead, we estimate the relative ratio by integrating Eq. (4) from $t = 0$ to ∞ [see Eq. (A6) in the Appendix] and using the physical constants in Table I. The result is shown in Fig. 8. Although there is an arbitrariness in the listed physical constants, the following conclusions can be drawn: at very low temperatures, the observed PL consists

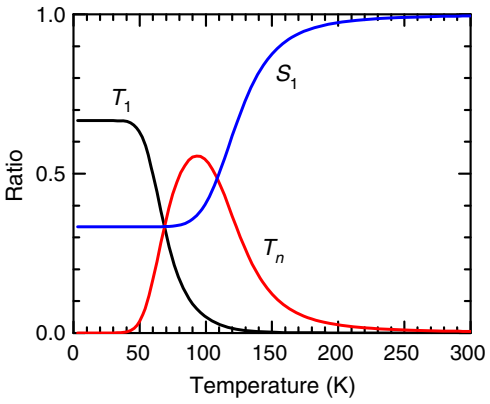

FIG. 8. Calculated result of relative intensity between a fluorescence component from S_1 and two phosphorescence components from T_n and T_1. This calculation is carried out using the four-level model and the physical constants listed in Table I, and we ignore any nonradiative decay channels into S_0.

of fluorescence from S_1 and phosphorescence from T_1; the former is emitted before the ISC process is completed. The major phosphorescence component from T_1 switches on at around 60 K, and the phosphorescence component from T_n is then maximized at around 100 K. Above 100 K, the phosphorescence component gradually decreases with increasing temperature. We would like to stress here that these conclusions are consistent with the observed PL spectral changes, although all of the physical constants used are obtained from the PL decay measurements.

It is also reasonable to inquire whether more triplet excited states exist between S_1 and T_1. From a four-level model, PL decay in the form of a sum of three exponential functions is expected. However, the observed PL decay curves cannot be reproduced, even with a sum of three exponential functions. From an m-level model, a temporal evolution in the form of a sum of $m-1$ exponential functions is obtained. Thus, the observed nonexponential PL decay curve might result from contributions of more triplet excited states in 4CzIPN. Here, we have found T_n from the analysis of the temperature dependence of the PL decay rates, but this method does not have a good energy resolution, particularly on the higher energy side. Thus, although we believe that the triplet excited state referred to as T_n is the second-lowest triplet excited state, we do not deny the possibility that an additional triplet excited state exists between S_1 and T_1. Rather, the fact that the narrower spectral shape of the phosphorescence from T_n and T_1 than that of the fluorescence from S_1 suggests the existence of an additional triplet excited state with a larger CT character, which is split from S_1 due to the exchange interaction. The existence of such a triplet CT excited state, nearly degenerate with S_1, was proposed by Ogiwara *et al.* from their time-resolved electron paramagnetic resonance measurements [18]. However, if such a triplet excited state exists, the determined energy gaps, $\Delta E_{T_n-T_1}$ and $\Delta E_{S_1-T_1}$, would only be slightly affected; the correction would be as small as the energy separation between the additional triplet excited state and S_1.

V. CONCLUSIONS

In this work, we show that T_n plays an important role in the decay process of excitons in 4CzIPN. To explain consistently the temperature dependences of the PL decay rates and the PL spectral shape, a four-level model consisting of S_1, T_1, T_n, and S_0 is needed. If a three-level model is applied, a wrong value for ΔE_{st} would be estimated and the phosphorescence component observed around 100 K would not be explicable. The analysis based on the four-level model described here can be used to identify an additional triplet excited state, i.e., T_n, which has recently become regarded as an important factor for fully understanding the reverse ISC mechanism. For the case of 4CzIPN, using the four-level mode, we determine that $\Delta E_{T_n-T_1} = 45 \pm 5$ meV and $\Delta E_{S_1-T_1} = 135 \pm 10$ meV. Recently, similar temperature

dependences of PL decay rates and PL spectra have been observed in other carbazolyl-dicyanobenzene-based TADF emitters [25], such as 1,2-bis(carbazol-9-yl)-4,5-dicyanobenzene and 1,4-dicyano-2,3,5,6-tetrakis(3,6-dimethylcarbazol-9-yl)benzene, which are known as 2CzPN and 4CzTPN-Me, respectively [2]. Therefore, contributions of T_n to emission properties are not a unique characteristic of 4CzIPN but rather appear to be common features of carbazolyl-dicyanobenzene-based TADF emitters.

ACKNOWLEDGMENTS

This work is supported in part by JSPS KAKENHI Grants No. 15H03883 and No. 15J12038, and by a Grant-in-Aid for Scientific Research on Innovative Areas "New Polymeric Materials Based on Element-Blocks (No. 2401)" (JSPS KAKENHI Grant No. 24102011).

APPENDIX: SOLUTIONS OF THE RATE EQUATIONS

The rate equations, Eq. (3), can be solved using the Laplace transform. In this appendix, we derive their solutions, which are used to calculate the temperature dependence of the decay rates and the relative ratios of the PL components. In a situation where the exciton-generation process is absent, $G = 0$, the rate equations are Laplace transformed as follows:

$$\begin{aligned} sX(s) - 1 &= (k_S + k_{\mathrm{ISC}n} + k_{\mathrm{ISC1}})X(s) + k_{\mathrm{RISC}n}Y(s) + k_{\mathrm{RISC1}}Z(s), \\ sY(s) &= k_{\mathrm{ISC}n}X(s) - (k_{T_n} + k_{\mathrm{IC}} + k_{\mathrm{RISC}n})Y(s) + k_{\mathrm{RIC}}Z(s), \\ sZ(s) &= k_{\mathrm{ISC1}}X(s) + k_{\mathrm{IC}}Y(s) - (k_{T_1} + k_{\mathrm{RISC1}} + k_{\mathrm{RIC}})Z(s), \end{aligned} \tag{A1}$$

where $X(s) = \mathcal{L}[S_1(t)]$, $Y(s) = \mathcal{L}[T_n(t)]$, and $Z(s) = \mathcal{L}[T_1(t)]$, and we assume $S_1(t) = 1$, $T_n(t) = 0$, and $T_1(t) = 0$ at $t = 0$ as the initial condition. By solving the simultaneous equations, Eq. (A1), we obtain

$$\begin{aligned} X(s) &= \frac{k_{\mathrm{IC}}(k_{\mathrm{RISC1}} + k_{T_1} + s) + (k_{\mathrm{RIC}} + k_{\mathrm{RISC1}} + k_{T_1} + s)(k_{\mathrm{RISC}n} + k_{T_n} + s)}{(k_1 + s)(k_2 + s)(k_3 + s)}, \\ Y(s) &= \frac{k_{\mathrm{RIC}}k_{\mathrm{ISC1}} + k_{\mathrm{ISC}n}(k_{\mathrm{RIC}} + k_{\mathrm{RISC1}} + k_{T_1} + s)}{(k_1 + s)(k_2 + s)(k_3 + s)}, \\ Z(s) &= \frac{k_{\mathrm{IC}}k_{\mathrm{ISC}n} + k_{\mathrm{ISC1}}(k_{\mathrm{IC}} + k_{\mathrm{RISC}n} + k_{T_n} + s)}{(k_1 + s)(k_2 + s)(k_3 + s)}, \end{aligned} \tag{A2}$$

where k_1, k_2, and k_3 are the solutions of the following cubic equation:

$$s^3 - as^2 + bs - c = 0, \tag{A3}$$

where

$$\begin{aligned} a &= k_S + k_{T_n} + k_{T_1} + k_{\mathrm{ISC}n} + k_{\mathrm{ISC1}} + k_{\mathrm{IC}} + k_{\mathrm{RISC}n} + k_{\mathrm{RISC1}} + k_{\mathrm{RIC}}, \\ b &= (k_{\mathrm{IC}} + k_{\mathrm{RISC}n} + k_{T_n})(k_{\mathrm{RIC}} + k_{\mathrm{RISC1}} + k_{T_1}) \\ &\quad + (k_S + k_{\mathrm{ISC1}} + k_{\mathrm{ISC}n})(k_{\mathrm{IC}} + k_{\mathrm{RIC}} + k_{\mathrm{RISC1}} + k_{\mathrm{RISC}n} + k_{T_1} + k_{T_n}) \\ &\quad - k_{\mathrm{RIC}}k_{\mathrm{IC}} - k_{\mathrm{ISC1}}k_{\mathrm{RISC1}} - k_{\mathrm{ISC}n}k_{\mathrm{RISC}n}, \\ c &= (k_{\mathrm{RIC}} + k_{\mathrm{RISC1}} + k_{T_1})(k_{\mathrm{IC}} + k_{\mathrm{RISC}n} + k_{T_n})k_S \\ &\quad + [k_{\mathrm{RIC}}k_{\mathrm{ISC1}} + k_{\mathrm{ISC}n}(k_{\mathrm{RIC}} + k_{\mathrm{RISC1}})]k_{T_n} \\ &\quad + [k_{\mathrm{IC}}k_{\mathrm{ISC}n} + k_{\mathrm{ISC1}}(k_{\mathrm{IC}} + k_{\mathrm{RISC}n})]k_{T_1} \\ &\quad + (k_{\mathrm{ISC}n} + k_{\mathrm{ISC1}})k_{T_n}k_{T_1} - k_{\mathrm{RIC}}k_{\mathrm{IC}}k_S. \end{aligned} \tag{A4}$$

Then, by taking the inverse Laplace transform of Eq. (A2), the solutions of the rate equations, Eq. (3), are

$$
\begin{aligned}
S_1(t) &= \frac{k_{\mathrm{IC}}(k_{\mathrm{RISC1}}+k_{T_1}-k_1)+(k_{\mathrm{RIC}}+k_{\mathrm{RISC1}}+k_{T_1}-k_1)(k_{\mathrm{RISC}n}+k_{T_n}-k_1)}{(k_2-k_1)(k_3-k_1)}e^{-k_1 t} \\
&+ \frac{k_{\mathrm{IC}}(k_{\mathrm{RISC1}}+k_{T_1}-k_2)+(k_{\mathrm{RIC}}+k_{\mathrm{RISC1}}+k_{T_1}-k_2)(k_{\mathrm{RISC}n}+k_{T_n}-k_2)}{(k_1-k_2)(k_3-k_2)}e^{-k_2 t} \\
&+ \frac{k_{\mathrm{IC}}(k_{\mathrm{RISC1}}+k_{T_1}-k_3)+(k_{\mathrm{RIC}}+k_{\mathrm{RISC1}}+k_{T_1}-k_3)(k_{\mathrm{RISC}n}+k_{T_n}-k_3)}{(k_1-k_3)(k_2-k_3)}e^{-k_3 t}, \\
T_n(t) &= \frac{k_{\mathrm{RIC}}k_{\mathrm{ISC1}}+k_{\mathrm{ISC}n}(k_{\mathrm{RIC}}+k_{\mathrm{RISC1}}+k_{T_1}-k_1)}{(k_2-k_1)(k_3-k_1)}e^{-k_1 t} \\
&+ \frac{k_{\mathrm{RIC}}k_{\mathrm{ISC1}}+k_{\mathrm{ISC}n}(k_{\mathrm{RIC}}+k_{\mathrm{RISC1}}+k_{T_1}-k_2)}{(k_1-k_2)(k_3-k_2)}e^{-k_2 t} \\
&+ \frac{k_{\mathrm{RIC}}k_{\mathrm{ISC1}}+k_{\mathrm{ISC}n}(k_{\mathrm{RIC}}+k_{\mathrm{RISC1}}+k_{T_1}-k_3)}{(k_1-k_3)(k_2-k_3)}e^{-k_3 t}, \\
T_1(t) &= \frac{k_{\mathrm{IC}}k_{\mathrm{ISC}n}+k_{\mathrm{ISC1}}(k_{\mathrm{IC}}+k_{\mathrm{RISC}n}+k_{T_n}-k_1)}{(k_2-k_1)(k_3-k_1)}e^{-k_1 t} \\
&+ \frac{k_{\mathrm{IC}}k_{\mathrm{ISC}n}+k_{\mathrm{ISC1}}(k_{\mathrm{IC}}+k_{\mathrm{RISC}n}+k_{T_n}-k_2)}{(k_1-k_2)(k_3-k_2)}e^{-k_2 t} \\
&+ \frac{k_{\mathrm{IC}}k_{\mathrm{ISC}n}+k_{\mathrm{ISC1}}(k_{\mathrm{IC}}+k_{\mathrm{RISC}n}+k_{T_n}-k_3)}{(k_1-k_3)(k_2-k_3)}e^{-k_3 t}.
\end{aligned}
\tag{A5}
$$

$S_1(t)$, $T_n(t)$, and $T_1(t)$ are all in the form of a sum of three exponential functions with the decay rates, k_1, k_2, and k_3. If nonradiative decay from S_1, T_n, and T_1 into S_0 is ignored, the relative intensities of PL emitted from S_1, T_n, and T_1 can be calculated by integrating $S_1(t)$, $T_n(t)$, and $T_1(t)$ from $t=0$ to ∞. The results are

$$
\begin{aligned}
\mathrm{PL}(S_1) &= \frac{k_{\mathrm{IC}}(k_{\mathrm{RISC1}}+k_{T_1}-k_1)+(k_{\mathrm{RIC}}+k_{\mathrm{RISC1}}+k_{T_1}-k_1)(k_{\mathrm{RISC}n}+k_{T_n}-k_1)}{k_1(k_2-k_1)(k_3-k_1)} \\
&+ \frac{k_{\mathrm{IC}}(k_{\mathrm{RISC1}}+k_{T_1}-k_2)+(k_{\mathrm{RIC}}+k_{\mathrm{RISC1}}+k_{T_1}-k_2)(k_{\mathrm{RISC}n}+k_{T_n}-k_2)}{k_2(k_1-k_2)(k_3-k_2)} \\
&+ \frac{k_{\mathrm{IC}}(k_{\mathrm{RISC1}}+k_{T_1}-k_3)+(k_{\mathrm{RIC}}+k_{\mathrm{RISC1}}+k_{T_1}-k_3)(k_{\mathrm{RISC}n}+k_{T_n}-k_3)}{k_3(k_1-k_3)(k_2-k_3)}, \\
\mathrm{PL}(T_n) &= \frac{k_{\mathrm{RIC}}k_{\mathrm{ISC1}}+k_{\mathrm{ISC}n}(k_{\mathrm{RIC}}+k_{\mathrm{RISC1}}+k_{T_1}-k_1)}{k_1(k_2-k_1)(k_3-k_1)} \\
&+ \frac{k_{\mathrm{RIC}}k_{\mathrm{ISC1}}+k_{\mathrm{ISC}n}(k_{\mathrm{RIC}}+k_{\mathrm{RISC1}}+k_{T_1}-k_2)}{k_2(k_1-k_2)(k_3-k_2)} \\
&+ \frac{k_{\mathrm{RIC}}k_{\mathrm{ISC1}}+k_{\mathrm{ISC}n}(k_{\mathrm{RIC}}+k_{\mathrm{RISC1}}+k_{T_1}-k_3)}{k_3(k_1-k_3)(k_2-k_3)}, \\
\mathrm{PL}(T_1) &= \frac{k_{\mathrm{IC}}k_{\mathrm{ISC}n}+k_{\mathrm{ISC1}}(k_{\mathrm{IC}}+k_{\mathrm{RISC}n}+k_{T_n}-k_1)}{k_1(k_2-k_1)(k_3-k_1)} \\
&+ \frac{k_{\mathrm{IC}}k_{\mathrm{ISC}n}+k_{\mathrm{ISC1}}(k_{\mathrm{IC}}+k_{\mathrm{RISC}n}+k_{T_n}-k_2)}{k_2(k_1-k_2)(k_3-k_2)} \\
&+ \frac{k_{\mathrm{IC}}k_{\mathrm{ISC}n}+k_{\mathrm{ISC1}}(k_{\mathrm{IC}}+k_{\mathrm{RISC}n}+k_{T_n}-k_3)}{k_3(k_1-k_3)(k_2-k_3)}.
\end{aligned}
\tag{A6}
$$

From the initial condition, $\mathrm{PL}(S_1)+\mathrm{PL}(T_n)+\mathrm{PL}(T_1)=1$.

[1] C. Adachi, Third-generation organic electroluminescence materials, Jpn. J. Appl. Phys. **53**, 060101 (2014).

[2] H. Uoyama, K. Goushi, K Shizu, H. Nomura, and C. Adachi, Highly efficient organic light-emitting diodes from delayed fluorescence, Nature (London) **492**, 234 (2012).

[3] A. Endo, M. Ogasawara, A. Takahashi, D. Yokoyama, Y. Kato, and C. Adachi, Thermally activated delayed fluorescence from sn^{4+}-porphyrin complexes and their application to organic light-emitting diodes—A novel mechanism for electroluminescence, Adv. Mater. **21**, 4802 (2009).

[4] A. Endo, K. Sato, K. Yoshimura, T. Kai, A. Kawada, H. Miyazaki, and C. Adach, Efficient up-conversion of triplet excitons into a singlet state and its application for organic light emitting diodes, Appl. Phys. Lett. **98**, 083302 (2011).

[5] M. N. Berberan-Santos and J. M. M. Garcia, Unusually strong delayed fluorescence of C_{70}, J. Am. Chem. Soc. **118**, 9391 (1996).

[6] C. Baleizão and M. N. Berberan-Santos, Thermally activated delayed fluorescence as a cycling process between excited singlet and triplet states: Application to the fullerenes, J. Chem. Phys. **126**, 204510 (2007).

[7] E. G. EcRae and M. Kasha, Enhancement of phosphorescence ability upon aggregation of dye molecules, J. Chem. Phys. **28**, 721 (1958).

[8] N. J. Turro, V. Ramamurthy, and J. C. Scaiano, *Modern Molecular Photochemistry of Organic Molecules* (University Science Books, Mill Valley, CA, 2010).

[9] J. R. Lakowicz, *Principles of Fluorescence Spectroscopy*, 3rd ed. (Springer, New York, 2010).

[10] F. B. Dias, K. N. Bourdakos, V. Jankus, K. C. Moss, K. T. Kamtekar, V. Bhalla, J. Santos, M. R. Bryce, and A. P. Monkman, Triplet harvesting with 100% efficiency by way of thermally activated delayed fluorescence in charge transfer OLED emitters, Adv. Mater. **25**, 3707 (2013).

[11] L. Yao, S. Zhang, R. Wang, W. Li, F. Shen, B. Yang, and Y. Ma, Highly efficient near-infrared organic light-emitting diode based on a butterfly-shaped donor-acceptor chromophore with strong solid-state fluorescence and a large proportion of radiative excitons, Angew. Chem. **126**, 2151 (2014).

[12] T. Sato, M. Uejima, K. Tanaka, H. Kaji, and C. Adachi, A light-emitting mechanism for organic light-emitting diodes: Molecular design for inverted singlet-triplet structure and symmetry-controlled thermally activated delayed fluorescence, J. Mater. Chem. C **3**, 870 (2015).

[13] F. B. Dias, J. Santos, D. R. Graves, P. Data, R. S. Nobuyasu, M. A. Fox, A. S. Batsanov, T. Palmeira, M. N. Berberan-Santos, M. R. Bryce, and A. P. Monkman, The role of local triplet excited states and D-A relative orientation in thermally activated delayed fluorescence: Photophysics and devices, Adv. Sci. **2016**, 1600080 (2016).

[14] C. M. Marian, Mechanism of the triplet-to-singlet upconversion in the assistant dopant ACRXTN, J. Phys. Chem. C **120**, 3715 (2016).

[15] J. Gibson, A. P. Monkman, and T. J. Penfold, The importance of vibronic coupling for efficient reverse intersystem crossing in thermally activated delayed fluorescence molecules, ChemPhysChem **17**, 2956 (2016).

[16] R. Ishimatsu, S. Matsunami, K. Shizu, C. Adachi, K. Nakano, and T. Imato, Solvent effect on thermally activated delayed fluorescence by 1,2,3,5-tetrakis(carbazol-9-yl)-4, 6-dicyanobenzene, J. Phys. Chem. A **117**, 5607 (2013).

[17] A. Niwa, T. Kobayashi, T. Nagase, K. Goushi, C. Adachi, and H. Naito, Temperature dependence of photoluminescence properties in a thermally activated delayed fluorescence emitter, Appl. Phys. Lett. **104**, 213303 (2014).

[18] T. Ogiwara, Y. Wakikawa, and T. Ikoma, Mechanism of intersystem crossing of thermally activated delayed fluorescence molecules, J. Phys. Chem. A **119**, 3415 (2015).

[19] H. Yoshida and K Yoshizaki, Electron affinities of organic materials used for organic light-emitting diodes: A low-energy inverse photoemission study, Org. Electron. **20**, 24 (2015).

[20] S. Wang, Y. Zhang, W. Chen, J. Chen, J. Wei, Y. Liu, and Y. Wang, Achieving high power efficiency and low roll-off OLEDs based on energy transfer from thermally activated delayed excitons to fluorescent dopants, Chem. Commun. (Cambridge) **51**, 11972 (2015).

[21] A. Niwa, K. Takaki, T. Kobayashi, T. Nagase, K. Goushi, C. Adachi, and H. Naito, Photoluminescence in a thermally activated delayed fluorescence emitter for organic light-emitting diodes, J. Imaging Soc. Jpn. **55**, 143 (2016).

[22] S. M. Menke and R. J. Holmes, Exciton transport in an organic semiconductor exhibiting thermally activated delayed fluorescence, J. Phys. Chem. C **120**, 8502 (2016).

[23] M. A. Baldo and S. R. Forrest, Transient analysis of organic electrophosphorescence: I. Transient analysis of triplet energy transfer, Phys. Rev. B **62**, 10958 (2000).

[24] K. Goushi, K. Yoshida, K. Sato, and C. Adachi, Organic light-emitting diodes employing efficient reverse intersystem crossing for triplet-to-singlet state conversion, Nat. Photonics **6**, 253 (2012).

[25] S. Haseyama, A. Niwa, T. Kobayashi, T. Nagase, K. Goushi, C. Adachi, and H. Naito (unpublished).